

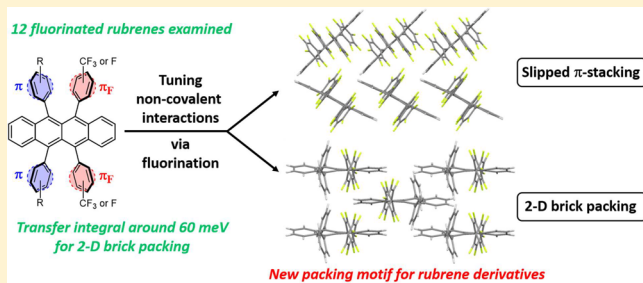
Partial Fluorination as a Strategy for Crystal Engineering of Rubrene Derivatives

William A. Ogden,[†] Soumen Ghosh, Matthew J. Bruzek,[§] Kathryn A. McGarry,[⊥] Luke Balhorn,[△] Victor Young, Jr., Lafe J. Purvis, Sarah E. Wegwerth, Zhuoran Zhang, Nicholas A. Serratore, Christopher J. Cramer,*[□] Laura Gagliardi,*[□] and Christopher J. Douglas*[□]

Department of Chemistry, Chemical Theory Center, and Supercomputing Institute, University of Minnesota, Minneapolis, Minnesota 55455, United States

Supporting Information

ABSTRACT: Through a close examination of the intermolecular interactions of rubrene (**1a**) and select derivatives (**1b–1p**), a clearer understanding of why certain fluorinated rubrene derivatives pack with planar tetracene backbones has been achieved. In this study we synthesized, crystallized, and determined the packing structure of new rubrene derivatives (**1h–p**). Previously, we proposed that introducing electron-withdrawing CF_3 substituents induced planarity by reducing intramolecular repulsion between the peripheral aryl groups (**1e–g**). However, we found that in most cases, further increasing the fluorine content of rubrene lead to twisted tetracene backbones in the solid state. To understand how rubrene (**1a**) and its derivatives (**1b–p**) pack in the solid state, we (re)examined the crystal structures through a systematic study of the close contacts. We found that planar tetracene cores occur when close contacts organize to produce an *S* symmetry element about a given rubrene molecule. We report the first instance of rubrene derivatives (**1l** and **1n**) that pack in a two-dimensional brick motif. The prospects for new rubrene derivatives in semiconductors were estimated by calculating the reorganization energies of the monomers and transfer integrals of the dimers we observed. Our work allows for the rational design and improved crystal engineering of new rubrene derivatives.



INTRODUCTION

Crystal engineering is a useful means to develop superior single-crystal organic semiconductors.^{1,2} To achieve high charge mobility in organic materials, molecular design must include (1) proper energy levels for hole or electron injections, and (2) solid state packing arrangements allowing for efficient intermolecular electronic coupling.^{3–7} Modification of the π -system by incorporating electron-donating or electron-withdrawing functional groups can often accomplish the first criterion.^{8–12} Predicting changes in crystal packing due to structural modifications, however, can be extremely difficult. In general, noncovalent intermolecular interactions, such as hydrogen bonding, halogen bonding, dipole–dipole, edge–face, and π – π stacking affect the packing motifs of a specific molecular system. These noncovalent interactions can be fine-tuned by alterations to the molecular structure including the extent of π interaction, incorporation of a heteroatom or a substituent, and steric bulk.^{13–17}

In designing organic molecules for semiconductors, fluorination is a popular strategy for altering electronics.^{18–20} Fluorine is often used as an isosteric substitution for hydrogen. Because of the difference in electronegativity, however, substitution of hydrogen with fluorine can have significant effects on both the physical and chemical properties of compounds.^{21–26} Perfluorination of a phenyl ring inverts the

electron density with respect to its non-fluorinated counterpart. Also, unlike ionic fluoride, which forms strong hydrogen bonds, organofluorine, C–F, forms comparatively weak hydrogen bonds.^{21–27} As a result, fluorination of an organic compound can increase its hydrophobic character. Because of this, organofluorine molecules form very few intermolecular interactions in solution. In the solid state, however, organofluorine molecules form intermolecular interactions that can significantly affect solid-state packing.^{28,29} In particular, organofluorine compounds make several types of intermolecular interactions, C–H…F, C–F…F, C–F… π , C–H… π_F , and π_F … π .^{21–26} Although individually these interactions tend to be relatively weak, organofluorine intermolecular interactions impart between –0.4 to –1 kcal/mol of stabilization per interaction, collectively they can produce significant changes in the crystal packing.^{30,31} In this work, we report a systematic study of functionalized rubrenes (Figure 1) in an attempt to better understand the underlying principles for crystal engineering of fluorinated rubrenes.

Rubrene (5,6,11,12-tetraphenyltetracene, **1a**) is a benchmark p-type organic semiconductor with a single crystal organic field-

Received: October 12, 2016

Revised: December 20, 2016

Published: December 29, 2016

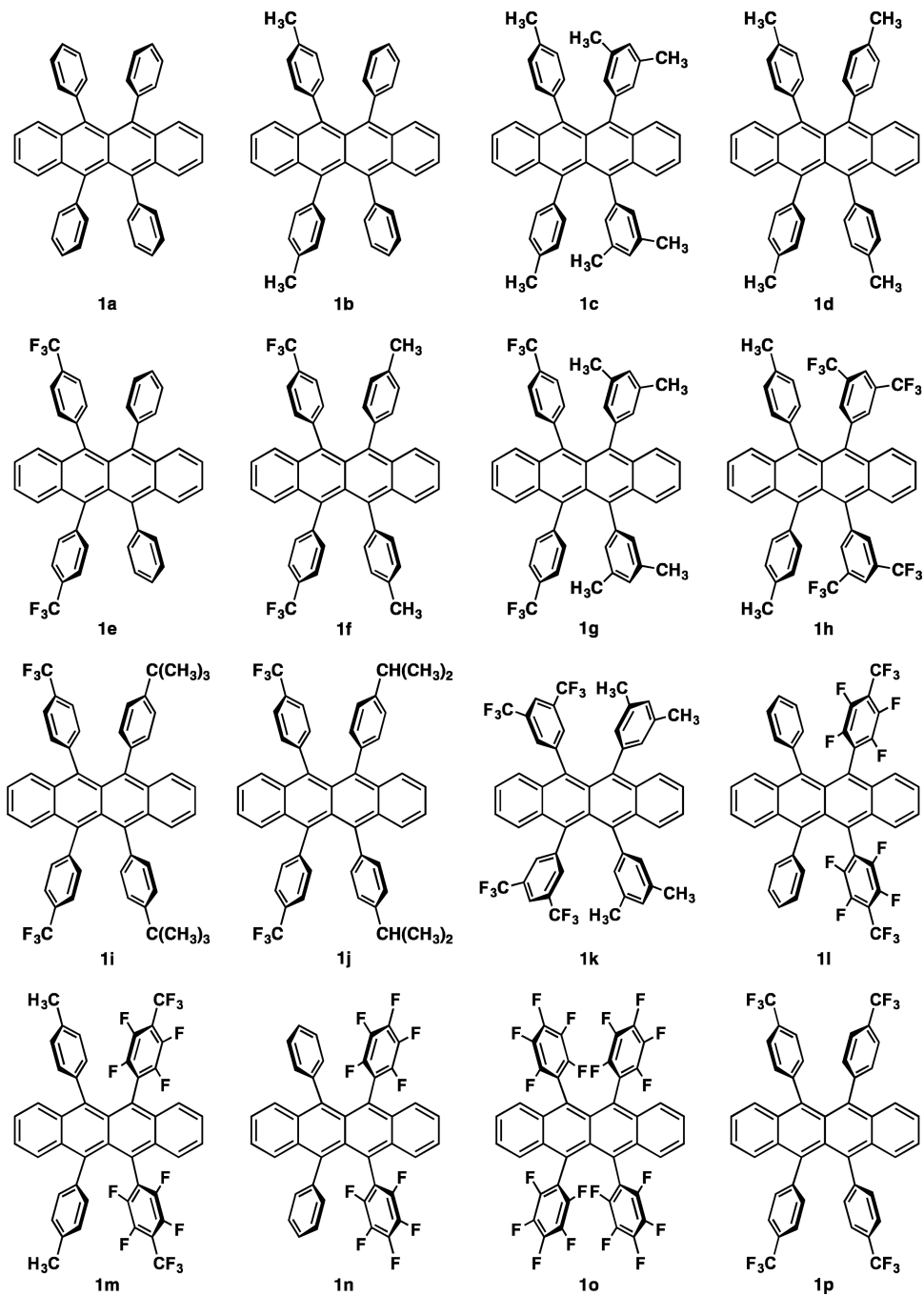


Figure 1. Rubrenes examined in this work.

effect transistor (SC-OFET) mobility of up to $40 \text{ cm}^2 \text{ V}^{-1} \text{ s}^{-1}$.^{32–37} The tight one-dimensional (1-D) slipped π -stack of the tetracene cores along the *b*-axis results in efficient charge transport in rubrene. Functionalizing the peripheral phenyls sometimes induces more desirable packing, such as tighter π -stacks, for increased mobility.^{38–42} Rubrene derivatives can also pack in different arrangements, with varying amounts of π -overlap. Rubrene itself displays three polymorphs (orthorhombic, monoclinic, and triclinic), of which only the orthorhombic possesses the packing needed for exceptional charge transport.⁴³ However, the planarity of the tetracene core, which is presumed necessary to achieve packing conducive to charge transport, is not always preserved in the solid state of rubrene derivatives.

On the basis of our previous work, which follows the work by Siegel et al., we believed that the intramolecular steric and electronic repulsion of the peripheral aryl groups forced into close proximity on the rubrene core caused the backbone to twist.^{38,44–48} Since our publication,³⁸ Brédas, Risko, and co-workers reported calculations that support the idea that isolated rubrene molecules (and derivatives) twist to reduce the unfavorable exchange–repulsion interaction between the peripheral aryl groups.⁴⁹ Theoretically, pairing electron-rich and electron-deficient peripheral aryl groups could mitigate unfavorable intramolecular interactions. This hypothesis appeared to have some merit based on our early success in crystal engineering of rubrenes. By incorporating a *para*-CF₃ group on two peripheral aryl groups (**1e–g**, Figure 1), we

Table 1. Synthesis of Rubrenes 1h–p

entry	Ar ¹	3, yield	Ar ²	1, yield ^a
1	3,5-(CF ₃) ₂ C ₆ H ₃	3a, 88%	4-CH ₃ C ₆ H ₄	1h, 42% ^b
2	3,5-(CF ₃) ₂ C ₆ H ₃		3,5-(CH ₃) ₂ C ₆ H ₃	1k, 70% ^b
3	4-CF ₃ C ₆ H ₄	3b, 91%	4-CF ₃ C ₆ H ₄	1p, 16% ^c
4	4-CF ₃ C ₆ H ₄		4-(t-Bu)C ₆ H ₄	1i, 44% ^c
5	4-CF ₃ C ₆ H ₄		4-(i-Pr)C ₆ H ₄	1j, 26% ^c
6	C ₆ H ₅	3c, 78%	C ₆ F ₅	1n, 60% ^b
7	C ₆ H ₅		4-CF ₃ C ₆ F ₄	1l, 40% ^b
8	4-CH ₃ C ₆ H ₄	3d, 93%	4-CF ₃ C ₆ F ₄	1m, 64% ^b

^aCombined yield for the two steps, organolithium addition and reduction of the resulting diol. ^bReduction with SnCl₂/HCl. ^cReduction with HI/Et₂O.

obtained rubrenes that packed similarly to orthorhombic rubrene with a planar backbone.³⁸

We now report that further fluorine substitution of the peripheral aryl groups results in rubrenes with twisted backbone conformations and different packing motifs. In our study, we examine inter- and intramolecular interactions of these new fluorinated rubrenes through a combination of computational studies, chemical synthesis, and X-ray crystallography. First, we prepared, crystallized, and obtained X-ray diffraction (XRD) data for a diverse set of fluorine-rich rubrenes. Next, we examined the energy barrier for the transition from a twisted to a planar backbone for a variety of fluorinated rubrenes, in an attempt to understand the planarization of rubrenes during crystallization. From the XRD data, we then attempted to correlate the amount of twist in the tetracene backbones and relate it to the steric bulk and/or electronics of the peripheral aryl groups. Our analyses led us to realize that fluorine-based intermolecular interactions played a more important role than intramolecular interactions in the backbone planarity and packing arrangements in single crystals of rubrenes **1e–p**. Thus, a careful examination of the close contacts was performed in an attempt to establish a correlation between the chemical structure and the crystal packing. Finally, we evaluated the prospects of selected substituted rubrenes as semiconductors by calculating the reorganization energies of the molecules and charge transport integrals based on the observed packing motifs.

EXPERIMENTAL SECTION

Synthesis. We prepared new rubrene derivatives **1h–n** and **1p** from dichloroquinone **2** following our previously reported route (Table 1).^{50–52} Rubrene **1o** required an alternate synthetic route, which is described in the discussion section.⁴⁰ Experimental procedures and tabulated characterization data for all new compounds are in the Supporting Information.

Crystallography. Rubrene derivatives were examined by single-crystal XRD using a Bruker-AXS D8 VENTURE CMOS PHOTON 100 diffractometer with an Incoatec IμS CuKα microfocus source ($\lambda = 1.54178 \text{ \AA}$) at 123 K for **1h–o** and Bruker APEX II Platform CCD diffractometer with graphite monochromator using MoKα radiation ($\lambda = 0.71073 \text{ \AA}$) at 173 K for **1p**. Reflections were integrated using the SAINT program. Absorption correction was performed using the SADABS program. Space group determination and data merge was performed using XPREP program. Structures were solved and refined with the APEX2 software. Hydrogen atoms were initially assigned

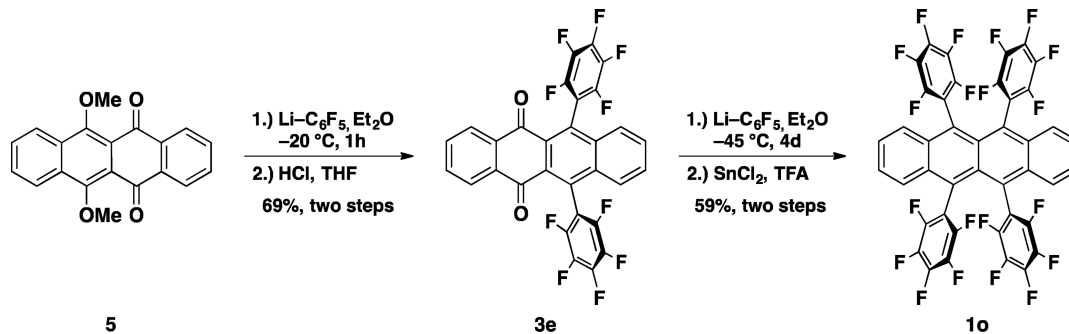
automatically by the geometric placement and refined as riding atoms. Fluorine atoms were assigned via q-peaks. Fluorine conformational disorder was determined by examining residual q-peaks. Rotational disorder in CH₃ groups was modeled using AFIX constraints, while CF₃ disorder was modeled by creating multiple C–F bonds, splitting them into parts and assigning fractional occupancy to each part. To correctly model fluorine conformational and rotational disorder, some geometric and displacement restraints and constraints were needed.

Crystal structures were analyzed using the Mercury program. All C–H bond distances were normalized to 1.083 Å.⁵³ Significant intermolecular interactions were defined as those within the van der Waals radii. Centroid distances reported herein represent geometrically averaged interaction distances for atoms shown to have multiple interaction to other atoms on a neighboring rubrene.

Hirshfeld analyses were performed using Crystal Explorer.⁵⁴ All van der Waals and covalent radii were set manually, hydrogen 1.20 and 0.37, fluorine 1.50 and 0.71, carbon 1.50 and 0.77 Å.

Computational Methodology. Monomers. We optimized the geometries of the flat and twisted conformations of rubrene and derivatives **1h** and **1k–o** in the gas-phase using the M06-L exchange-correlation density functional and the 6-31G(d,p) basis set.⁵⁵ Also, we optimized the geometries of the twisted and flat conformations of the corresponding radical cations and radical anions. Vibrational frequency analyses confirmed the nature (minimum or transition-state (TS) structure) of all stationary points. We define the planarization energy as the (positive) energy difference between the flat and twisted backbone conformers. We scanned the dihedral/twist angle δ from 0 to 60° by intervals of 5° while optimizing all other internal coordinates to compute the barriers for the interconversion of the two conformers. Untwist energies and interconversion barrier heights were also calculated for the M06-L geometries with the M06⁵⁶ and ωB97XD⁵⁷ functionals and the 6-31G(d,p) basis set. All calculations on monomers made use of the Gaussian 09 suite of electronic structure programs.⁵⁸

Transfer Integrals. We used dimer models to elucidate the transfer of holes and electrons through different packing arrangements of separate rubrene molecules. First, we extracted these dimer models from available crystal structures (Figure S1). The π -stacked dimer (PD) and herringbone dimer (HD) models were extracted from the crystal structure of **1f**. The twisted π -stacked dimer (TPD) and twisted herringbone dimer (THD) models were obtained from the crystal structures of derivative **1l** and derivative **1h**, respectively. The experimental crystal packing structures of compounds **1l** and **1n** have two distinct TPD dimers possessing different overlaps and distances between the monomers. We named them TPD1 and TPD2. The slipped herringbone dimer (SHD) model was obtained from the crystal structure of derivative **1o**, and the slipped π -stacked dimer (SPD) model was obtained from the rubrene crystal structure in

Scheme 1. Synthesis of F₂₀-Rubrene 1o

triclinic phase. Subsequently, we constrained the positions of the atoms in the tetracene backbones while optimizing the peripheral aryl groups with appropriate substituents. We kept the intermolecular distance constant for all rubrene derivatives within a particular dimer model so as to separate substitution effects on the electronic structure from any effects on minimum-energy dimer geometry. Such an approach is further justified insofar as many dimer geometries are not local minima in the absence of a crystal lattice to enforce local orientation. Constrained optimizations employed the PBE functional and double- ζ Slater-type orbital basis sets containing one polarization function (DZP).⁵⁹ Damped dispersion effects were included with the pairwise D3⁶⁰ correction of Grimme et al. and the damping function of Becke and Johnson.⁶¹

Following optimization of the dimer geometries, charge transfer integrals were calculated at the PBE0⁶²/DZP level of theory using the fragment molecular orbital (FMO)⁶³ approach. In this approach, we constructed the dimer Fock matrix in the basis of monomer orbitals. Off-diagonal elements of the Fock matrix are $t_{mn} = \langle \varphi_m | h_{KS} | \varphi_n \rangle$, where φ_i represents the fragment molecular orbitals and i represents the sites (m or n). For the matrix elements relevant to the hole (or the electron) transfer integral between the m th and n th sites in a system, φ_m and φ_n are the HOMOs (or LUMOs) of the m th and n th site, respectively. In our dimer model, sites represent individual monomers and h_{KS} is the Kohn–Sham Fock operator.⁶⁴ Diagonal elements of the Fock matrix are, $\epsilon_i = \langle \varphi_i | h_{KS} | \varphi_i \rangle$. S_{mn} is the overlap matrix element between orbital φ_m and φ_n . Since the Fock matrix is constructed here by using nonorthogonal monomer orbital basis, the effective transfer integral (t_{mn}^{eff}) is calculated using the formula

$$t_{mn}^{\text{eff}} = \frac{t_{mn} - \frac{1}{2}(\epsilon_m + \epsilon_n)S_{mn}}{1 - S_{mn}^2} \quad (1)$$

All these calculations on dimers were carried out with the Amsterdam Density Functional suite of electronic structure programs.⁶⁵ Full details associated with computing transfer integrals in ADF are provided in the references.^{63,64}

RESULTS AND DISCUSSION

Synthesis. Over the years, many routes to prepare rubrene derivatives have been developed.^{38–40,66–69} Our route allows for late-stage diversification of the edge phenyl substituents at positions 5, 6, 11, and 12 of the tetracene core. Suzuki–Miyaura coupling of dichloroquinone **2** with *para*- or *meta*-substituted arylboronic acids provided diarylquinones **3a–d** in good yields (78–93%, Table 1). We then installed a second pair of aryl substituents by addition of aryl lithium reagents to quinones **3a–d**. The resulting diols formed as mixtures of diastereomers that we carried on directly into reduction with either HI/Et₂O or stannous chloride/HCl to avoid decomposition of the diols. We purified the final rubrene products **1h–p** by precipitation and subsequent recrystallization. The final two steps of this sequence provided the partially

fluorinated rubrene derivatives in 16–70% yield. In some cases, the use of the SnCl₂/HCl procedure minimized the formation of byproducts obtained under the HI/Et₂O conditions. The major byproduct under HI/Et₂O conditions resulted from closure of the diol to a [2.2.1] oxygen bridged ring system.⁷⁰ Often, these oxo-bridged byproducts precipitated from the reaction mixtures as colorless solids.

The synthesis of rubrene derivative **1o** with *peri*-perfluorophenyl groups required a modified synthesis (Scheme 1). Our attempts at Suzuki–Miyaura coupling of dichloride **2** with pentafluorophenyl boronic acid failed. We recognized that a double Stork–Danheiser type addition/rearrangement sequence might accomplish the synthesis of quinone **3e**.⁷¹ Treatment of 6,11-dimethoxytetracene-5,12-dione (**5**)⁷² with pentafluorophenyl lithium,⁷³ followed by treatment of the resulting diol with HCl provided quinone **3e** in 69% yield over the two steps. Addition of the second set of perfluorophenyl rings also proved quite challenging. After extensive experimentation, we settled on treating quinone **3e** with pentafluorophenyl lithium in Et₂O at –45 °C for 4 days. The prolonged reaction time at this temperature proved the best compromise between a sluggish reaction at –78 °C and extensive decomposition at temperatures higher than –45 °C. We heated the resulting mixture of diastereomers with SnCl₂ and trifluoroacetic acid to yield rubrene **1o** in 59% yield over the two steps.

Limited Influence of Intramolecular Interactions on Solid-State Conformation. To date, most planar rubrene derivatives have packed in a herringbone motif (Figure 2).^{3,37}

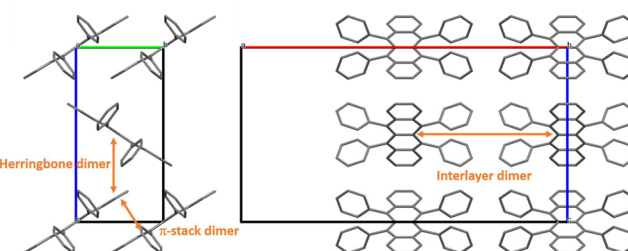


Figure 2. Definition of dimers discussed in this paper, intralayer (left) and interlayer (right), using the unit cell of rubrene **1a**.

However, the factors promoting crystallization of planar rubrene conformers, and derivatives, are not well understood from a purely experimental perspective. Further complicating the analysis, both planar and twisted rubrenes pack in a variety of motifs. To better understand the conformation-controlling factors in fluorinated rubrene derivatives, we began by

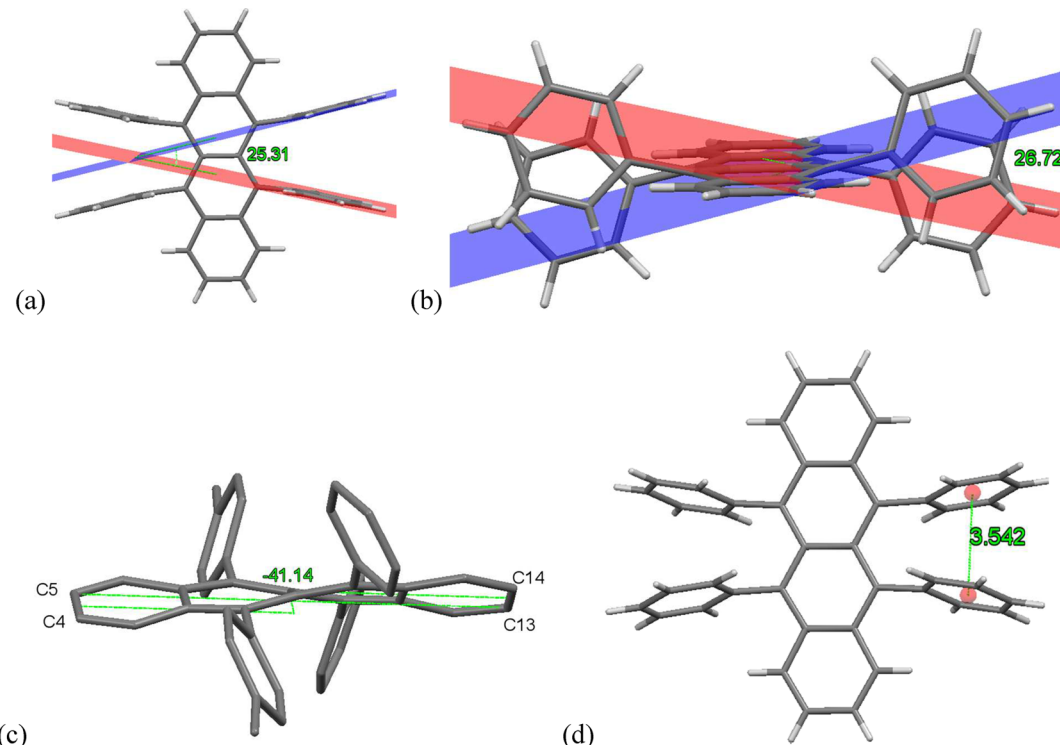


Figure 3. Example measurement of structural parameters: (a) splay angle, (b) slip angle, (c) backbone twist, (d) centroid-to-centroid distance. Note: Several of the rubrene derivatives, both flat and twisted, were found to have “puckering” along the tetracene backbone as well (Figure S3).

Table 2. Crystal Data of Rubrene Derivatives 1a–b, 1e–h, 1k–m, 1o

compound	1a	1b	1e	1f	1g	1h	1k	1l	1m	1o
crystal system ^a	O	O	O	O	O	M	M	M	M	T
space group	<i>Cmca</i>	<i>Pna2</i> ₁	<i>Pnma</i>	<i>Pbcm</i>	<i>Pbcm</i>	<i>P2</i> ₁ / <i>c</i>	<i>P2</i> ₁	<i>C2/c</i>	<i>P2</i> ₁ / <i>n</i>	<i>P</i> ₁
twist (degrees)	molecule 1 molecule 2 ^b	0 41.2	0 0	0 0	0 19.9	19.9 39.5	39.5 40	28.9 28.4	28.4 0	0 0
centroid-to-centroid distance (Å)	molecule 1 molecule 2 ^b	3.54 3.44/3.75 ^c	3.43 3.43	3.42 3.47	3.47 3.38/3.43 ^c	3.38/3.43 ^c 3.45/3.43 ^c	3.45/3.43 ^c 3.45/3.42 ^c	3.4 3.34/3.41 ^c	3.33 3.39	
aryl splay angle (deg)	molecule 1 molecule 2 ^b	25.3 29.2/16.3 ^c	18.5 18.2	18.5 18.5	18.5 23.1/19.1 ^c	17.5/18.8 ^c 16.6/19.9 ^c	23.3 18.5	18.6/13.7 ^c 31.5/34.1 ^c	13.7 28.3	17 30.3
aryl slip angle (deg)	molecule 1 molecule 2 ^b	26.7 45.3/34.1 ^c	23.2 24.7	30.8 30.8	24.5/26.9 ^c 34.0/34.3 ^c	34.0/34.3 ^c 36.3	18.5 36.3			

^aO = orthorhombic, M = monoclinic, T = triclinic. ^bMolecule 2 indicates two molecules in the asymmetric unit. ^cIndicates values are inequivalent across the tetracene core. A description of how values were measured for each parameter can be found in the Supporting Information with Table S3.

reevaluating our prior hypothesis that reducing the torsional strain of the peripheral aryl groups would lead to planar rubrenes in the solid state.

It is a common practice to influence molecular conformation by tuning intramolecular interactions when studying rubrenes and other organic semiconductors.^{74–78} On the basis of our previous work,³⁸ the electronic component of our hypothesis seemed to have some merit. Rubrenes **1b–d**, with only methyl group substitutions, exhibited twisted backbones in the solid state. By replacing a methyl with an electron-withdrawing CF₃ group (**1e–g**) we obtained planar backbones. The steric portion of our hypothesis appeared less important. For example, rubrene **1f**, sterically analogous to **1d**, was planar. The planarity in **1f** suggested that the addition of bulky groups

to the peripheral aryl groups was not the primary factor affecting backbone planarity in the solid state. Calculations from the Brédas⁴⁹ group further downplayed sterics. Their results indicated that unfavorable exchange-repulsion interactions between the peripheral aryl groups caused the tetracene cores of rubrenes to twist. In designing our new rubrene targets, we worked under the hypothesis that we could obtain a planar tetracene core by reducing the exchange-repulsion of the peripheral aryl groups through incorporation of electron-withdrawing substituents. New fluorinated rubrenes **1h–p** were prepared and crystallized based on this hypothesis. In most instances, however, further decreasing the electron density on the peripheral aryl groups resulted in rubrenes that packed with a twisted backbone instead of the desired planar backbone.

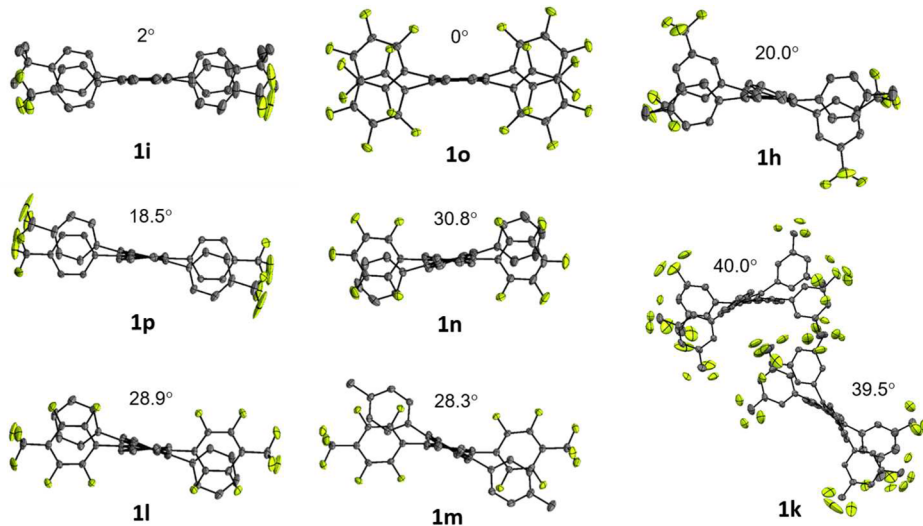


Figure 4. Thermal ellipsoid plots of rubrene **1h–i**, **1k–o**, showing backbone twist angles. For **1k**, two twist angles are observed.⁸²

To probe the limitations of our working hypothesis, we applied density functional theory (DFT) to compare the relative energies as well as the energetics of interconversion between twisted and planar backbones for rubrenes **1h** and **1k–o**. As observed by others, these calculations confirmed that, for isolated rubrene molecules, the twisted conformation is the lowest energy state for all derivatives.^{49,79} More interestingly though, our calculations showed that converting from a planar to a twisted tetracene core is essentially a barrierless process (Table S1). To estimate the energetic penalty associated with crystallizing planar rubrenes, we then examined the energy cost for planarization of rubrenes (Table S2). All electron deficient rubrenes have a lower energy barrier to planarization than **1a**. Although the DFT model generally agreed with our prior experimental results,³⁸ we could not correlate intramolecular electronics or sterics and planarization energies with our new rubrenes (Table S2). For example, **1h** is less sterically encumbered than **1k**, but **1h** has a higher planarization energy. Interestingly, the planarization energy is the highest for the parent rubrene (**1a**) even though it is the least sterically congested and known to adopt a planar backbone in several single crystal polymorphs. Since we were unable to explain our experimental results in conjunction with computational data on the planarization energies, we looked for alternative ways to relate the backbone twist to substituent effects.

No rubrene derivative crystallizes with the peripheral aryl groups perfectly eclipsed. Instead, rings can splay (Figure 3a) or slip past each other (Figure 3b); in extreme cases, the whole tetracene backbone twists (Figure 3c) to reduce the repulsion. We measured each of these phenomena for each rubrene derivative (Table S3) and summarized values for selected rubrene derivatives in Table 2. Our analysis of the data found no direct correlations between the degree of electron deficiency of the peripheral aryl groups with any one parameter (splay, slide, or twist). We also found no correlation between the splay and slide angles with backbone twist or among each other. In an attempt to simplify the analysis, we examined the centroid-to-centroid (CtC) distances (Figure 3d) of the peripheral aryl groups. If twisting of the backbone resulted in relieving the repulsion of the peripheral aryl groups, we would expect a correlation between the CtC distance and the degree of backbone twist. We found no such correlation. The CtC

distances occur over a very small range (3.33–3.75 Å) among all derivatives. We observe no trend relating the degree of backbone twist or electron deficiency of the peripheral aryl groups. Having failed to correlate backbone twist with electronics, we re-examined steric influences.

To examine the effect of intramolecular steric interactions of the peripheral aryl groups with the observed twist, we started with those containing *para* substitutions. The introduction of CH₃ groups, as in **1b**, induces a high degree of twisting, 41.2° and 42.8°. However, upon substitution of the CH₃ with CF₃, **1e**, a planar backbone is observed. This suggests sterics at the *para* position are not a major contributor since the van der Waals volume of CH₃ is 16.8 Å³ while CF₃ is 42.6 Å³.⁸⁰ Additionally, substituting the CH₃ group for a *t*-butyl group (**1i**, which displays a 2° backbone twist) or and isopropyl group (**1j**, a planar tetracene backbone) had minimal impact on planarity.

The effect of substitution at other positions is more complex. The identity of the groups at the *meta* positions seems to have more impact than the *para* groups. By comparing the crystal structures of **1g** and **1h**, we found that switching the position of CF₃ and CH₃ groups resulted in a significant backbone conformation change from planar (**1g**) to twisted (**1h**, 20.0°). Again, sterics do not explain the backbone twist observed upon replacing hydrogen with isosteric fluorine. For example, rubrenes **1e** and **1f** are both planar, while **1l** and **1m** are both twisted, 28.9° and 28.4° respectively. Taken as a whole, we cannot find any correlation between the planarity in the tetracene backbone and intramolecular interactions of the peripheral aryl groups.

From our computational studies, the twisted conformation is lower in energy in the gas phase by 1.7–3.5 kcal/mol (Table S2). Aside from intramolecular steric and electronic factors, intermolecular interactions also impact each conformer's energy level within a crystal lattice: as reasoned by others,⁴⁹ these additive intermolecular interactions could be more decisive in the crystallization of a given rubrene conformer. Furthermore, if intramolecular interaction of the peripheral aryl groups dictated solid state conformation of the tetracene backbone, then one would not expect to observe two symmetry independent conformers in the asymmetric unit. For example, the crystal structures of **1d** and **1k** contain two molecules in the asymmetric unit, each molecule with a twisted tetracene core,

42.8° and 33.9°, 39.5° and 40.0° respectively. Additionally, Tokito and co-workers report a furan-containing rubrene derivative that has two molecules in the asymmetric unit where one has a twisted core, 35.8°, and the other is planar, with no overlap of the tetracene cores.⁸¹ Therefore, to explain why some rubrene derivatives planarize, we turned to a close examination of the intermolecular interactions within the crystals.

Intermolecular Interactions Influence on Solid-State Conformation. In our rubrene derivatives, C–F···X intermolecular interactions quickly begin to dominate as more fluorines are added. From our current study, we believe that the backbone conformation and packing motif observed in **1e–p** result from noncovalent intermolecular C–F···X interactions of CF₃ and/or aryl fluorides (C–F) with other groups. These C–F···X interactions appear to be as significant or more significant than the observed C–H···π (−1 to −3 kcal/mol), C–H···H (−0.4 kcal/mol), and π···π (−1 to −3 kcal/mol) interactions, which would otherwise be decisive, as seen in other acene crystal structures.^{83–86} Below, we will only discuss intermolecular interactions within the van der Waals radii to examine the influence of the interactions on molecular conformation and crystal packing.

To gain a frame of reference for interactions that may be necessary to stabilize a planar core, we revisited the crystal structure of parent rubrene, **1a**.⁸⁷ Notably, the closest interactions within the π-dimer are symmetric C–H···H, 2.189 Å at 142.2° between a set of phenyl *ortho* hydrogens and the edge hydrogens of the tetracene core (Figure 5a).

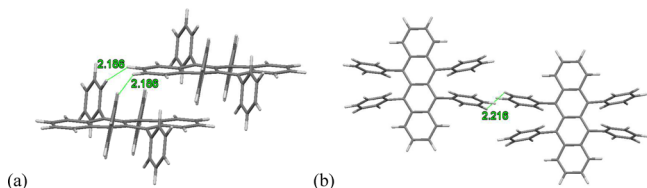


Figure 5. Intermolecular interactions of (a) intralayer dimers and (b) interlayer dimers in rubrene **1a**.

Across the interlayer (Figure 5b), neighboring *meta* hydrogens form a short contact, C–H···H 2.216 Å, between the peripheral aryl groups. From our analysis of **1a**, we observed that intermolecular C–H···H interactions between the intralayer dimers and across the interlayer (Figure 5) appear to stabilize crystal packing of the planar rubrene conformer. We noticed symmetric interactions on both sides of a given rubrene molecule in the lattice. This led us to conclude that these counter balancing interactions stabilize the otherwise higher energy planar conformation. Additionally, Brédas' computational study suggested that interactions within the intralayer neighbors significantly contribute to stabilization of planar π-stacking rubrenes.⁴⁹ Brédas also concludes that interlayer interactions are more significant for stabilizing the *overall* crystal lattice. On the basis of this understanding, we then examined how the introduction of substituents on the peripheral aryl groups enhanced and/or disrupted these key interactions necessary to align both the intra- and interlayers.

Beginning with **1e–g**, which all have a planar tetracene core, we worked on identifying additional interactions that influence the crystal packing. For **1e** and **1f**, C–H···π interactions form the closest short contacts to the core, but the *ortho* hydrogens of the peripheral phenyl or *para*-tolyl groups were found to

contact a nearby core in the herringbone dimer, as well as the π-dimer (Figure 6). Similarly, Sassella and co-workers observed

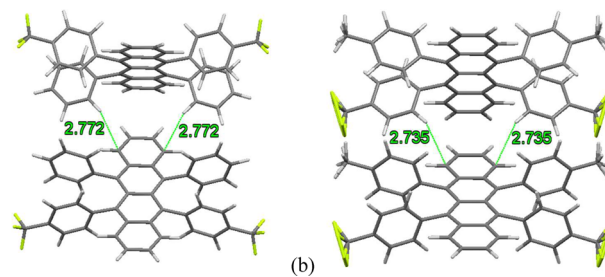


Figure 6. Intermolecular interactions between the herringbone dimers in **1e** (a) and **1f** (b).

ortho C–H···π and C–H···H interactions in planar substituted rubrenes.⁸⁸ While **1g** does form long *ortho* C–H···H to the π-stacked dimer, the closest short contacts are not to the tetracene core, yet the tetracene core is planar. In **1e–g**, groups at the *para* position forge the interlayer interactions, instead of the groups at the *meta* position (**1a**). Interlayer interactions (Figure 7) for **1e** are stabilized by symmetric C–F···H

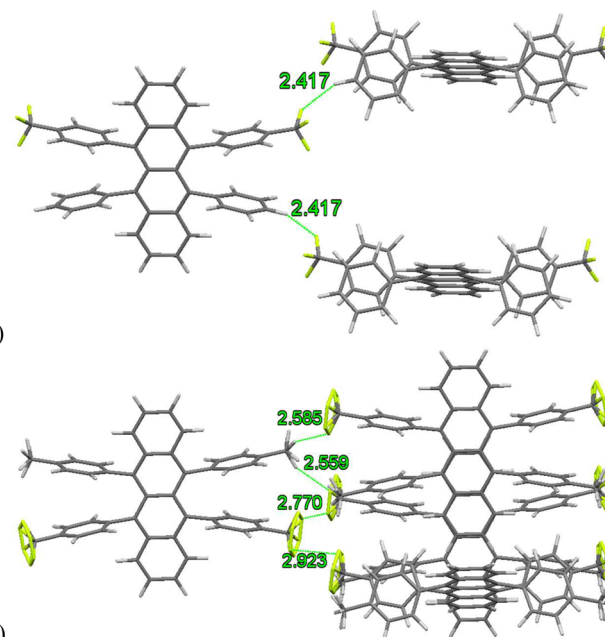


Figure 7. Interlayer interactions in **1e** (a) and **1f** (b).

interactions between *para*-CF₃ and *para*-hydrogen at 2.417 Å at an angle of 140.94°. Because of rotational disorder of both the *para*-CF₃ and the *para*-methyl groups, **1f** displays C–F···H interactions of 2.585 (132.25°) and 2.559 Å (167.01°) as well as C–F···F interactions at 2.770 (148.17°) and 2.923 Å (102.07°) between the *para* substituents. Compound **1g** has a C–F···H at 2.448 Å (114.04°) with the *para*-hydrogen and C–H···H at 2.185 Å between *meta*-CH₃ groups. *Para*-CF₃ substituents form the interlayer interactions by enabling the formation of favorable C–F···X interactions.

As a comparison, we reexamined the interactions found in substituted rubrenes **1b–d** which all have a twisted tetracene core (41.2°, 30.3°, and 42.8°/33.9° respectively). In these derivatives, C–H···π interactions were found to dominate the

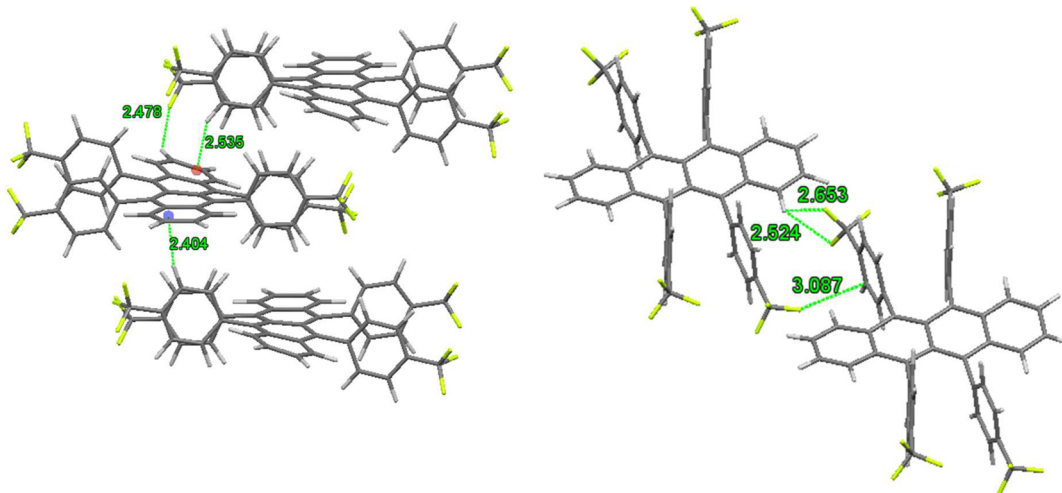


Figure 8. Intermolecular interactions in rubrene 1p.

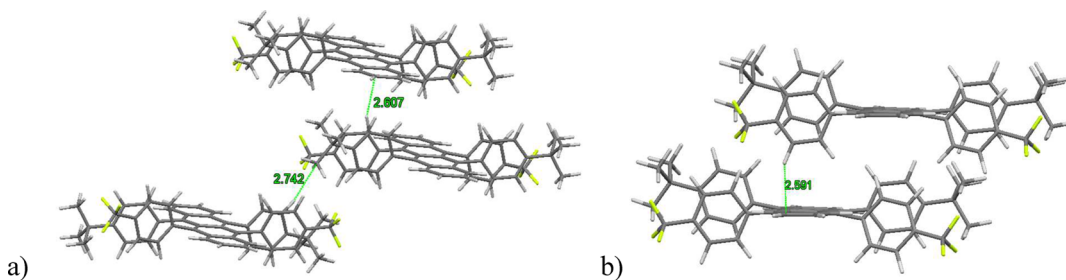


Figure 9. (a, b) Intermolecular interactions in rubrene 1l.

close contacts. The absence of π -stacking in **1b-d** complicates direct comparison to **1e-f**, but inferences can still be made. For example, in **1b** (molecular structure analogous to **1e**) an *ortho*-hydrogen of an unsubstituted peripheral aryl group forms a C–H \cdots π interaction at 2.692 Å with a methyl substituted peripheral aryl group instead of the tetracene core. Additionally, the *ortho*-hydrogen of the peripheral tolyl group forms a C–H \cdots H interaction at 2.250 Å with a neighboring *para*-CH₃. In **1b**, a *meta*-hydrogen of the *para*-CH₃ peripheral aryl group forms a C–H \cdots π interaction of 2.640 Å, C15–C14 centroid, with a tetracene core and a C–H \cdots H interaction of 2.346 Å. In **1c**, the methyl groups at the *meta* positions have close contacts with several other regions of neighboring molecules. A methyl of a peripheral *meta*-xylyl group displays C–H \cdots π interactions with C9, C10, and C16 of a neighboring tetracene core. Across the tetracene core, each methyl group of the other peripheral *meta*-xylyl form different close contacts to neighboring molecules. Finally, **1d**, in which all the peripheral aryl groups contain *para*-CH₃ groups, is complicated by containing two molecules in the asymmetric unit. From the XRD, we observed that C–H \cdots π interactions dominate the close contacts between the two molecules in the asymmetric unit, the closest being 2.457 Å, C2–C3–C7 centroid contact between tetracene cores. The majority of remaining short contacts involve the methyl substituents (Table S7). Overall, the introduction of methyl groups at either the *para* or *meta* positions favor interactions with the tetracene core rather than forming interactions across the interlayer with other peripheral aryl groups. Comparing the solid state interactions of **1a-g** suggests that stabilizing the planar conformation of rubrene in the solid state requires forming symmetric intermolecular interactions about the planar

conformer. Also, all the planar rubrenes (**1a**, **1e-g**, and others⁸⁸) show a symmetric peripheral aryl group slip, via an S-like symmetry element, resulting from symmetric interlayer interactions.

To further explore the effects of *para*-CF₃ substitution, we examined **1p** that possesses *para*-CF₃ on each peripheral aryl group. These additional CF₃ groups had a dramatic effect on the packing. Instead of a herringbone, it has a monoclinic C2/c crystal structure with no π -stacking. Additionally, the core has an 18° twist with slipped 1-D packing along the short axis. The slipped 1-D packing shows C–H \cdots π interactions between the *meta*-H and the tetracene core. Symmetric interactions are observed on the top and bottom face of the core; however, along the tetracene backbone they are not equivalent. On one end of the tetracene core a C–H \cdots π interaction of 2.404 Å, C9–C9'-C10–C17 centroid,⁸⁹ is observed, while on the other end a longer C–H \cdots π distance of 2.535 Å, C2–C2'-C1 centroid, is seen (Figure 8, see Supporting Information for additional diagrams of these contacts). Unlike the previous rubrenes, the *para* substituents form C–F \cdots H interactions with the tetracene core. On one end, a fluorine forms interactions with C2–H (2.478 Å) and on the other with C10–H (2.524 and 2.653 Å) of the tetracene core.⁸⁹ The fluorine also forms an interlayer interaction with a *meta*-carbon of a peripheral aryl group. The additional CF₃ groups appear to have disrupted interlayer interactions of the *para* groups that were observed above in **1e-g** as a means to align the tetracene backbones analogously to rubrene **1a**. When comparing **1e-g** and **1p**, the interlayer of **1e-g** arranges to align electron-poor and electron-rich peripheral aryl groups to form interactions that orient the packing in the solid state. While in rubrene **1p**, the CF₃ groups

interacted with the core, in seeking an electron-rich donor, which drastically altered the packing. In combination with the observations from above, we hypothesize that the ability to order the interlayer by forming fluorine-based interactions can be influential in helping to stabilize a planar core.

Extending this analysis to new *para*-CF₃ rubrene derivatives, examination of **1i**, with a bulky *t*-butyl group at the *para* position, has a slight twist of 2° with a π-stacked packing motif slipped along the short axis of the tetracene (Figure 9a,b). Rather than the *ortho*-H···π interactions that were observed in rubrenes **1a** and **1e–f**, a C–H···π interaction between a *meta*-H of a *para*-CF₃ peripheral aryl group with C3 (2.591 Å) and a *meta*-H of the *t*-butyl peripheral aryl group with C9 (2.607 Å)⁸⁹ are observed on opposite sides of the tetracene core. Similar to **1e–g**, the electron-rich and electron-poor rings align across the interlayer. However, because of the bulkiness of the *t*-butyl group, a methyl of the *t*-butyl group interacts with the *meta*-H on a *t*-butyl peripheral aryl group (2.742 Å), rather than CF₃. Overall, this is an interesting case where a nearly planar rubrene does not display π-stacking, but instead the intermolecular interactions on the tetracene core are well balanced to give only a slight twist in the tetracene core. The unit cell for **1j** was determined to be primitive monoclinic with cell constants $a = 15.2600(5)$ Å, $b = 13.8935(4)$ Å, $c = 18.1133(6)$ Å, $\beta = 99.371(1)$ °, and $V = 3789.0(2)$ Å³. The space group was determined to be $P2_1/c$ with $Z = 4$. The structure solution found two, one-half occupied molecules each located on unique inversion centers. Early solution and refinement attempts led to a pathological model, whereby the –CF₃ and –CH(CH₃)₂ moieties were 50:50 disordered. No suitable model could be attained where all compositionally disordered moieties could be refined with appropriate restraints and constraints. There were indications that the center of mass of the two molecules were displaced slightly away from the crystallographic inversion center. Reducing the apparent true space group symmetry to either Pc or $P2_1$ only created a more unstable refinement. The best residual achieved was $R_i = 0.09$ with significant remaining problems. No crystallographic data beyond this description will be included with this report.

Introduction of CF₃ groups to *meta* positions, **1h** and **1k**, resulted in rubrenes with twisted backbones (20° and 40° respectively) and different packing motifs (sandwich herringbone and slipped 1D packing, respectively). Examining the core of **1h**, on one side of the mirror plane along the tetracene unit, the π-stack dimers still have one C–H···H interaction between an *ortho* hydrogen on a *para*-tolyl peripheral aryl group and the neighboring tetracene core (2.138 Å *para*-CH₃, Figure 10). Additionally, an *ortho* hydrogen on a di-*meta*-CF₃ peripheral aryl group displays a close contact to the same neighboring tetracene core (2.157 Å, *meta*-CF₃), but this C–H···H interaction is at an angle much more acute than the analogous close contact in rubrene **1a**. On the other side, all the short contacts are with the herringbone dimer. The CF₃ groups at the *meta* position are able to reach both the tetracene core and the peripheral aryl groups, forming several C–F···H and C–F···F interactions. These different C–F···X interactions cause an imbalance of interactions on the rubrene, disrupting the intra- and interlayer ordering observed in rubrenes **1e–g**. Consequently, the planar tetracene conformation is not achieved. Similar to **1j**, the high degree of disorder in **1k** only allowed for limited data analysis; therefore, while the crystal structure and data are present, a thorough analysis of intermolecular interactions could not be undertaken.

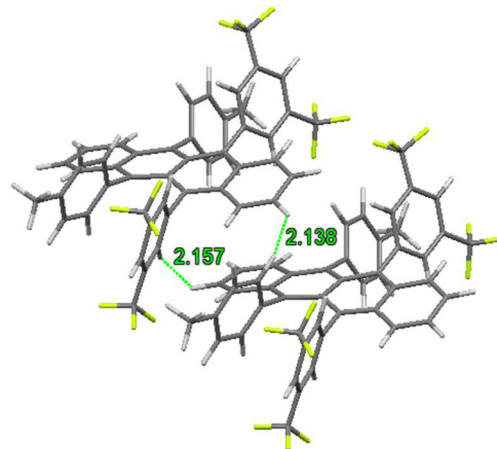


Figure 10. Intermolecular interactions in rubrene **1h**.

We also examined the replacement of the hydrogen atoms in **1e** and **1f** with fluorine atoms, to give *para*-heptafluorotolyl groups, as in **1l** and **1m**. Perfluorination of the peripheral *para*-tolyl groups led to a monoclinic $C2/c$ crystal structure with 2-D brick packing for **1l** and a backbone twist of 28.9°.^{5,15–17} The 2-D brick packing is assembled by *ortho* fluorines and *ortho* hydrogens of the peripheral aryl groups interacting with the tetracene backbone of a neighboring molecule (Figure 11a). The π-stack distances are slightly different at either end of the tetracene core, 3.622 and 3.525 Å. In rubrene **1l**, the closest interactions are C–F···H interactions. The C–F···H interactions occur within the π-stacked dimers, between tetracene C2–H and *ortho* fluorine atoms both above and below at 2.594 (141.61°) or 2.433 Å (125.08°) (Figure 11b). We also observed intralayer C–F···H interactions between *ortho* fluorine atoms, both above and below the plane, and the C9–H (2.346 Å, 148.45°).⁸⁹ Additionally, intralayer C–H···H interactions are also observed, again, between *ortho* hydrogen and C9–H and C10–H of the tetracene core. The interlayer is again connected by pairing the electron-rich and electron-poor peripheral aryl groups through C–F···H interactions (2.573 Å, 119.50° and 2.555 Å, 123.10°, Figure 11c) of the CF₃ group with the *meta* hydrogen. Conversely, in rubrene **1m** both the *para*-CH₃ and the *meta* hydrogen of the tolyl group interact with the CF₃ group altering the packing motif. The *ortho* fluorine atoms of the peripheral aryl groups now interact with the neighboring tetracene cores in an edge-to-edge manner (Figure 12). The *para*-CH₃ is also observed to form C–F···H interactions with *meta* fluorine atoms of a neighboring molecule. Overall, these observations lead us to conclude that fluorine substituted rubrenes pack so as to maximize fluorine-based interactions. Also, in comparison with rubrene **1e–g**, it appears that *meta*-fluorine substituents form C–F···X interactions that can disrupt favorable intralayer and interlayer interactions necessary for planar rubrene conformers in the solid state.

The last two rubrene derivatives, **1n** (twisted backbone 30.8°) and **1o** (planar backbone), have perfluorophenyl substituents. Rubrene **1n**, with perfluoro and unsubstituted phenyls, has triclinic $P\bar{1}$ with 2-D brick packing, similar to **1l**. Again, the *ortho* fluorine and *ortho* hydrogen atoms interact with the tetracene core, orienting the π-stacked dimer (Figure 13a), manifesting in the 2-D brick packing of **1l** and **1n**. Similar to **1l**, the π-stack distances for **1n** are slightly different at either end of the tetracene core, 3.609 and 3.514 Å. The tightest interactions are C–F···H between π-stacked rubrenes (Figure

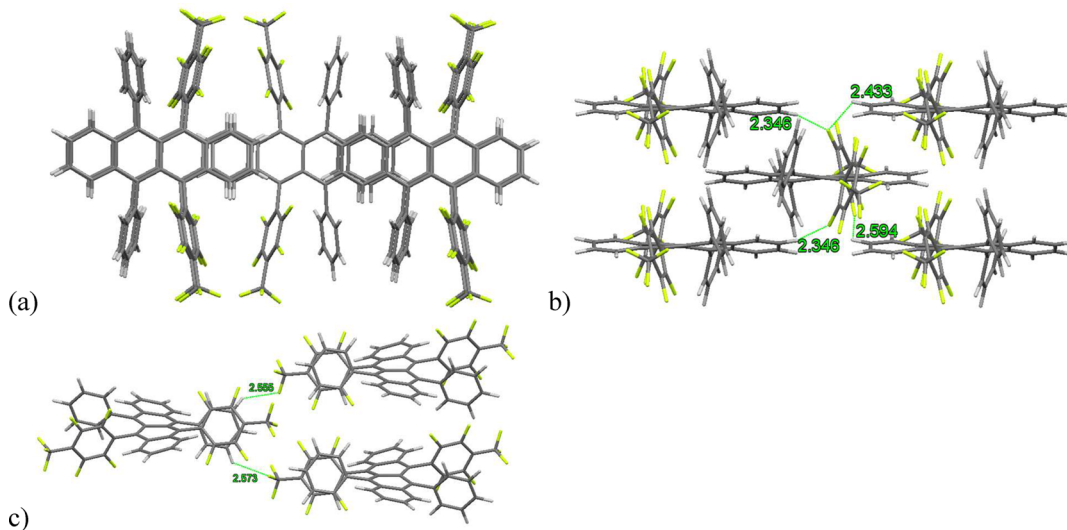


Figure 11. Crystal packing of rubrene **1l**, show (a) the π -stacking of the 2-D brick, (b) intermolecular interactions between π -stack dimers, (c) intermolecular interactions of the interlayer.

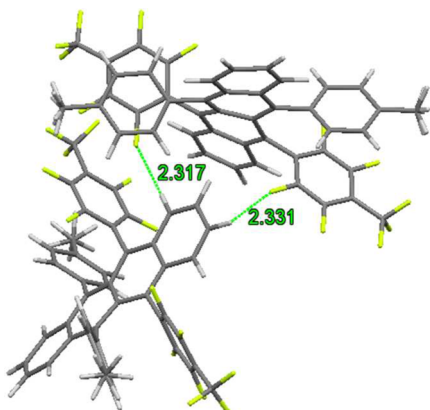


Figure 12. Intermolecular interactions in rubrene **1m**.

13b). As in **1l**, the interlayer dimers **1n** align in a highly ordered manner so that the phenyl and perfluorophenyl groups can efficiently pack with each other via C–F···H interactions (Figure 13c, 2.346–2.584 Å, angles listed separately in Table S16). Rubrenes **1l** and **1n** are extremely interesting because they are the first derivatives observed to pack in a 2-D brick motif. Computational models, as well as transport experiments, demonstrate improved charge transport of 2-D brick packing motif over 1-D herringbone or π -stacked herringbone due to decreased charge transport anisotropy.^{90–92} This opens a new crystal packing motif to target for crystal engineering of single crystal rubrenes: planar 2-D brick.

Rubrene derivative **1o** packs in a slipped herringbone motif with a planar tetracene backbone. We observed two molecules in the asymmetric unit with two distinct distances for the π -stacked dimers. The difference in π -dimer distance, 3.632 and 5.562 Å (Figure 14), is a result of a π – π_F interaction between

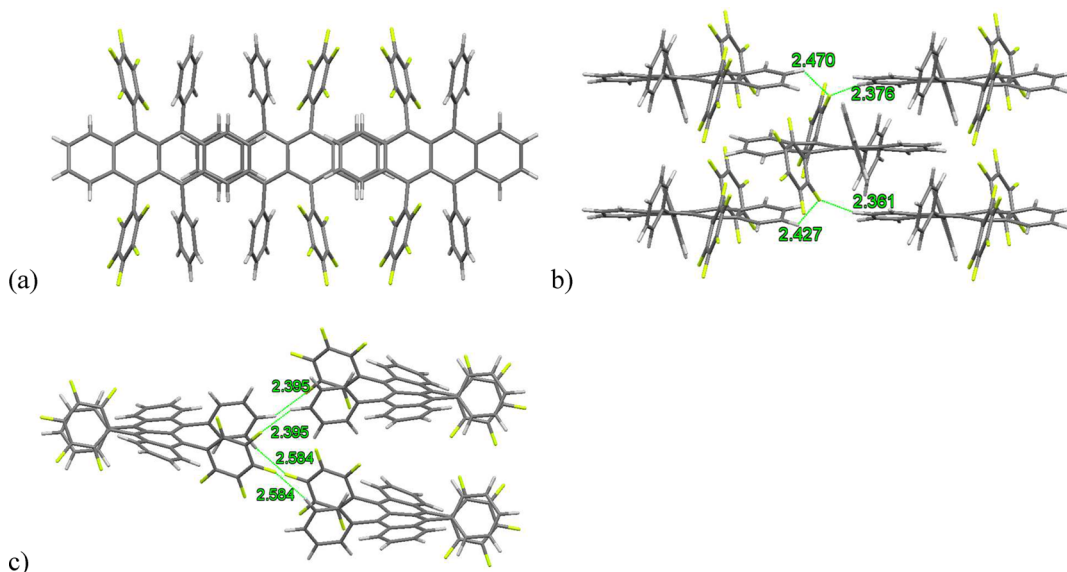


Figure 13. Crystal packing of rubrene **1n**, show (a) the π -stacking of the 2-D brick, (b) intermolecular interactions between π -stack dimers, (c) intermolecular interactions of the interlayer.

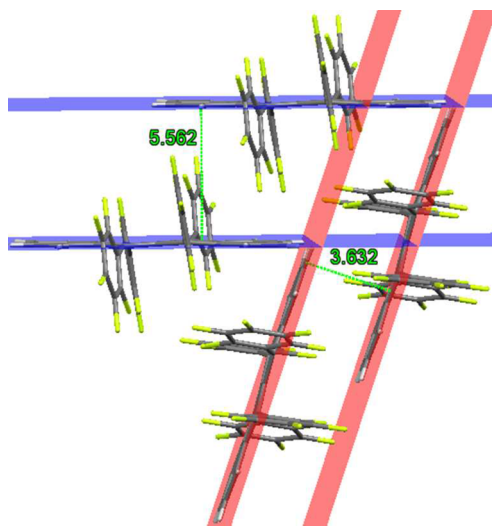


Figure 14. Rubrene **1o** π -stacked dimer distances. Red and blue areas indicate planes containing the tetracene cores.

neighboring herringbone dimers pushing one set of π -dimers apart (Figure 15b). Similar to **1l** and **1n**, the tightly bound π -

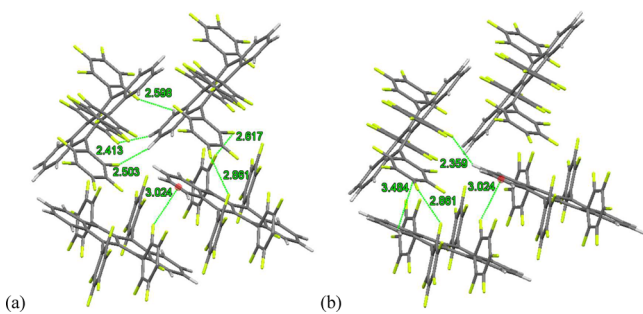


Figure 15. Packing arrangements and fluorine-based interactions in rubrene **1o**, (a) intralayer close contacts are highlighted, (b) shows additional intralayer close contacts including $\pi\cdots\pi_F$ and type II C–F...F interactions.

stacked dimers (3.632 \AA) form three *ortho*-fluorine C–F...H interactions: C10–H (2.598 \AA , 154.41°), C2–H (2.503 \AA , 146.31°), and C9–H (2.413 \AA , 131.91°).⁸⁹ While in the other π -stacked dimer, C–F... π interactions occur between *ortho* fluorine and the tetracene core (3.024 \AA , C2A–C1A centroid). Rubrenes **1e**–**n**, all contain the so-called type I C–F...F interactions; however, in **1o** we also observe the rare type II C–F...F interactions between the herringbone dimers (Figure 15).^{21–26} As in **1a**, **1f**, **1g**, and others, we observed that for both molecules in the asymmetric unit, the interactions along the tetracene backbone contain an inversion symmetry, resulting in planarity.⁸⁸

Through our analysis of rubrenes **1a**–**p**, we have demonstrated the importance of symmetric intermolecular interactions in stabilizing and crystallizing the planar rubrene conformations. We have noted the need to consider all types of intermolecular interactions, even weak C–F...X interactions, when engineering rubrene derivatives for solid-state organic electronic devices. Through the analysis of crystal structures **1a**–**p**, we observed that intermolecular interactions between the *ortho* positions and the tetracene core help to orient the π -stacking dimer as well as the herringbone dimers. Also, symmetric interactions of the peripheral aryl groups stabilize

the higher energy planar conformation of rubrene and its derivatives via the interlayer interactions of *para* fluorine and *meta* or *para* hydrogens groups (Table 3).

Table 3. Position of Key Short Contacts on Peripheral Aryl groups

	rubrene	intralayer	interlayer	π -stacked dimer distance \AA
herringbone (planar)				
	1a	<i>ortho</i> H	<i>meta</i> H	3.66
	1e	<i>ortho</i> H	<i>para</i> H and <i>para</i> F	3.55
	1f	<i>ortho</i> H	<i>para</i> H and <i>para</i> F	3.51
	1g	<i>ortho</i> H	<i>para</i> H, <i>meta</i> H	3.63
	1o	<i>ortho</i> F, <i>meta</i> F	<i>para</i> F	3.63 and 5.56
slipped 1-D (slightly twisted)	1i	<i>meta</i> H	<i>para</i> F, <i>meta</i> H	NA
2-D brick (twisted)	1l	<i>ortho</i> H, <i>ortho</i> F	<i>para</i> F, <i>meta</i> H	3.62 and 3.53
	1n	<i>ortho</i> H, <i>ortho</i> F	<i>para</i> F, <i>meta</i> H	3.61 and 3.51
other twisted	1h	<i>ortho</i> H, <i>meta</i> F	<i>para</i> H, <i>meta</i> F	NA
	1m	<i>para</i> H	<i>para</i> H, <i>para</i> F, <i>meta</i> H	
	1p	<i>para</i> F, <i>meta</i> H	<i>para</i> F	

Hirshfeld Surface Analysis. To further support the significance of the intermolecular interactions identified above, Hirshfeld analysis was performed for each rubrene derivative, **1b**–**p**. Hirshfeld analyses readily identify the shortest intermolecular interactions and the significance of each interaction based on the packing observed in a crystal structure. Its usefulness has been demonstrated for a wide range of molecules, including rubrenes.^{42,93,94} In the first part of the analysis, a Hirshfeld surface (HS) is generated where color coding is used to indicated the closeness of the contact. Red represents close contacts inside the van der Waal radii, white represents close contacts near or at the van der Waals radii, and blue represents close contacts outside the van der Waals radii. In the second part, a fingerprint plot is color coded to show the significance of each specific contact. Blue represents a small contribution of the close contact to the packing in the solid state, while green to red represents significant contribution of the close contacts to the solid-state packing. Only a select number of Hirshfeld surfaces (HSs) and 2-D fingerprint plots are discussed here, while all rubrene derivatives can be found in the Supporting Information (Figures S4–S18).

Bergantin and Moret have previously reported the HS and 2-D fingerprint of rubrene **1a**.⁴² As observed from the crystal structure, the HS readily highlights the close contacts between the *ortho* hydrogen and the hydrogens of the tetracene core in the π -stacked dimer, as well as between the *meta* hydrogens of the peripheral aryl groups across the interlayer. Extending this methodology to one of our planar rubrenes, we examined **1f**. In agreement with our analysis above, the HS shows close contacts at the *ortho* hydrogen of the peripheral aryl group and the tetracene core in the π -stacked dimer, as well as across the interlayer at *para* CF₃ and *para* methyl groups of the peripheral aryl groups. However, from the HS it is more readily evident

that the π -stacked dimer interactions are weaker (white) than the interlayer interactions (red). In examining the 2-D fingerprint plot, it is clear that the C–F…H form strong interactions and make a significant number (>20%) of the intermolecular interactions observed in the crystal packing of **1f**, Figure 16. C–F…H interactions comprise of 25.5% of the interactions observed in the solid state, C–F…F interactions 5%.

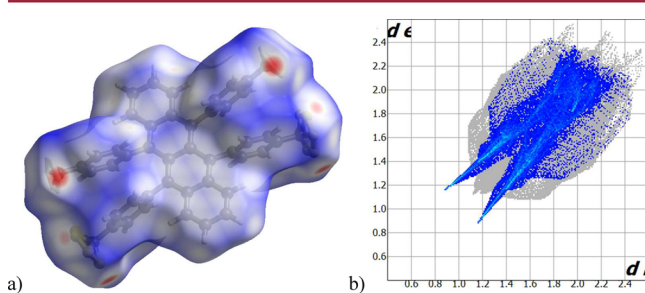


Figure 16. (a) Hirshfeld surface, (b) C–F…H interactions 2-D fingerprint plots of rubrene **1f**.

For rubrene **1p**, as observed in our geometric analysis of close contacts, the HSs plot show close contacts that occur between *meta* hydrogen of the peripheral aryl groups and the teracene core, Figure 17a. C–F…H interactions close contacts

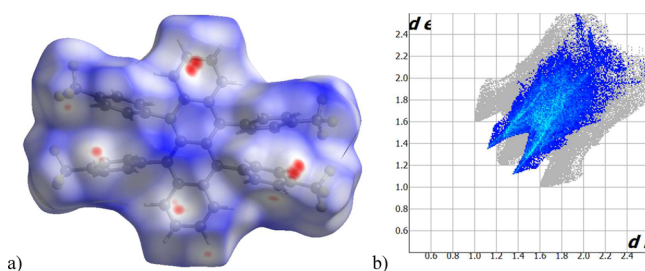


Figure 17. (a) Hirshfeld surface, (b) 2-D fingerprint plots of rubrene **1p**.

can also be seen at the *para* CF₃ and the tetracene core of a neighboring rubrene. The 2-D plot again shows a significant number of C–F…H interactions, Figure 17b. C–F…H interactions now comprise 43.2% of the close contacts interactions observed in the solid state, close contacts C–F…F 6.8% and C–F…C 5.7%.

Similarly, the HS of rubrene **1n** exhibits close contacts at both the *ortho* hydrogen and *ortho* fluorine to the tetracene core in the π -stacked dimer. Now though, as indicated by the red surface, these interactions are stronger. Also observed are close contacts between *meta* hydrogen and *meta* fluorine, and of *para* hydrogens and *para* fluorines in the interlayer. The 2-D fingerprint plot of C–F…H interactions in the crystal structure of **1n**, Figure 18, now comprise of 45.3% of the close contacts interactions observed in the solid state, C–F…F interactions 9.8% and C–F…C interactions 3%.

The Hirshfeld analysis of C–F…X interactions corroborates the single crystal analysis of short contacts discussed above and significance of the different intermolecular interactions that occur at the *ortho*, *meta*, and *para*, position of the peripheral aryl rings.

Although we have targeted the packing motif that theory has suggested is optimal for charge transport in single-crystal

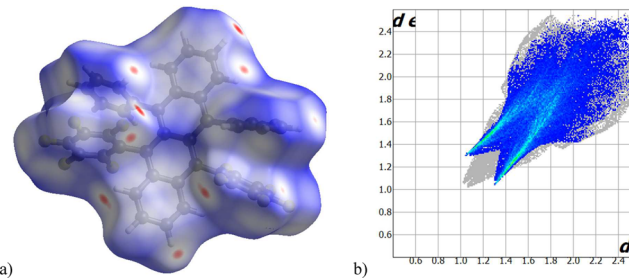


Figure 18. (a) Hirshfeld surface, (b) C–F…H interactions 2-D fingerprint plots of rubrene **1n**.

devices, i.e., slipped π -stacking in orthorhombic rubrene,³⁷ we observed new packing motifs not previously observed in other rubrene derivatives. Qualitatively, several of these, particularly those packing with 2-D brick motifs, may have overlap of neighboring tetracene cores conducive to charge transport. To better assess the potential of these new packing motifs, we turned to chemical theory and computational modeling.

Charge Transport Properties of Rubrene Derivatives.

According to Marcus theory (eq 2), the rate constant (k) for electron (e) or hole (h) transport in organic semiconductors is dependent on the Gibbs free energy (ΔG°) of electron or hole transfer, the transfer integral (t) between the initial and final states, and the reorganization energy (λ). Because of the anisotropic packing of rubrene, ΔG° is taken to be zero as the two sites are chemically and electronically identical. The efficiency of charge transport is therefore dependent on the reorganization energy and transfer integral, both of which can be estimated using computational chemistry, beginning with looking at reorganization energies.

$$k_{h/e} = \frac{2\pi}{\hbar\sqrt{4\pi\lambda_{h/e}k_B T}} t_{h/e}^2 \exp\left(-\frac{(\lambda_{h/e} + \Delta G^\circ)^2}{4\lambda k_B T}\right) \quad (2)$$

Reorganization energies were calculated by considering two contributions separately: relaxation energy of the newly charged species and relaxation energy of the newly uncharged species. Calculated reorganization energies of electron and hole transfer for **1a**, **1h**, and **1k-o** are presented in Table 4. As found for neutral rubrene, the charged rubrenes have two local minimum-energy structures in which the backbone is either twisted or planar. In all cases, the cationic rubrenes have a lower reorganization energy, and therefore all the derivatives should act as hole transport semiconductors. Interestingly, the twisted

Table 4. Reorganization Energies (meV) Predicted for Various Rubrene Derivatives in Their Flat and Twisted Molecular Conformations^a

molecule	hole reorganization energy		electron reorganization energy	
	flat	twisted	flat	twisted
1a	136	135	208	183
1n	151	159	199	180
1o	156	183	192	189
1l	153	158	257	241
1m	195	164	252	220
1k	162	168	235	207
1h	177	174	249	220

^aM06-L/6-31G(d,p).

backbone is lower in energy for all the rubrene derivatives for both anionic and cationic species. Also, it is notable that the difference in reorganization energy between the planar and twisted backbone conformers is small, which suggests that charge transport can readily occur through rubrenes with either a planar or twisted backbone.

Charge Transfer Models. Next, we calculated the charge transfer integrals using dimer models based on crystal packing and unit cells determined from rubrene and its derivatives. The smallest possible model that can be used to compute transfer integrals is a dimer model. We took into account the existence of several different packing motifs for two adjacent molecules based on those found via solved crystal structures of rubrene and its derivatives (Figure S1). We considered dimer models where the tetracene core is planar or twisted (as discussed in the Experimental Section).

The calculated effective hole and electron transfer integrals for rubrene and its derivatives (**1h** and **1k–o**) for different possible dimer models determined for single crystals among PD, TPD, HD, THD, SHD, and SPD (terms defined in the methodology section) configurations are presented in Figures 19 and 20. Results for all dimer model calculations for rubrene

electron transfer, the π -stacked dimer had the greatest transfer integral due to their high level of π overlap. The values for the PD models also confirm that transfer integral values are fairly insensitive to the structure of the peripheral aryl groups so long as the same packing is preserved. The TPD1 configuration, containing two monomers with twisted tetracene backbones, had the lowest value for hole transfer integral. The TPD2 type configuration is only found in **1l** and **1n**, and although it also has two monomers with twisted tetracene backbones like TPD1, the distance between those monomers is smaller and there is a greater overlap between tetracene backbones of two monomers. TPD2 gives the second highest transfer integral values (Figure 19). There are modest variations in hole transfer integral values for all other geometries, with SHD generally providing maximal or near maximal values within the set; all, however, are at least a factor of 5 smaller than predicted for the PD geometry (Figures 19 and S19).

A very similar trend to that for the hole transfer integrals was found for the effective electron transfer integrals (Figures 20 and S20). The larger calculated value for the PD configuration, compared to all others, is indicative of how strongly the two π systems interact in the PD orientation. Interestingly, when a dimer model was considered with rubrene (**1a**) molecules containing twisted backbones having identical parameters as the planar model (PD), computed effective hole and electron transfer integrals were found to be 86.6 and 100.1 meV, respectively. Also, for the 2-D brick, the TPD2 model gives transfer integrals of around 60 meV for **1l** and **1n**. It indicates that this new packing motif may be a viable alternative to the herringbone packing motif for charge transport in rubrene. This shows that the differences in calculated transfer integral values, and the ability to transport charge, between PD and TPD arise from the greater intermolecular distance and smaller π overlap between tetracene backbones, not due to the twisting of tetracene backbones.

CONCLUSION

The analysis of the crystal structures of fluorinated rubrenes **1e–p** clearly shows that C–F…X intermolecular interactions play a major role in determining molecular conformation and crystal packing. Analysis of the crystal structures, along with computational results, indicates that in order to stabilize the higher energy planar rubrene conformation, symmetric intermolecular interactions in the crystal structure are needed. Comparing the crystal structures of **1a–p**, it is clear that intermolecular interactions between the *ortho* positions and the tetracene core help to orient the π -stacking dimer. At the same time, interlayer interactions are important for stabilizing the planar rubrene. When adding new functional groups to the peripheral aryl groups consideration must be made for both new interactions formed as well as interactions that are disrupted. For rubrene derivatives, as more fluorines are added to the molecule, C–F…X intermolecular interactions quickly dominate, which can disrupt π -stacking and planarity. For fluorinated rubrenes, **1l**, **1n**, and **1o**, the fluorine at the *ortho* position of the peripheral aryl groups interacted strongly with the tetracene core to orient the rubrene molecules in the intralayer and help stabilize the π -stacking. Addition of fluorine groups to the *para* position appear to help stabilize the higher energy planar conformation of rubrene derivatives, **1e–g**, and **1o**. These stabilizing interactions are formed through the ordering of the interlayer, which pairs electron-rich and electron-deficient peripheral aryl groups, allowing for favorable

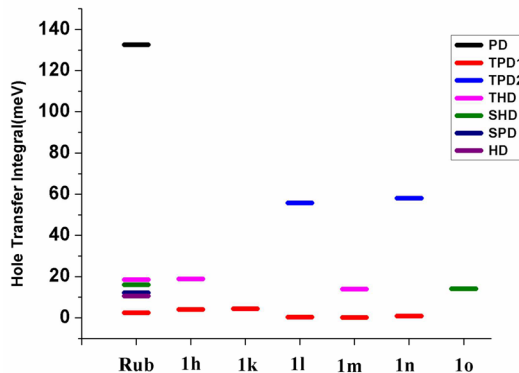


Figure 19. Absolute values of effective hole transfer integrals (meV, PBE0/DZP) for parent rubrene and derivatives (**1h** and **1k–o**) for dimer models PD, TPD1, TPD2, HD, THD, SHD, and SPD.

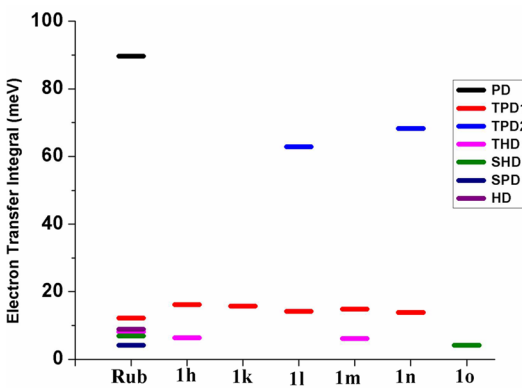


Figure 20. Absolute values of effective electron transfer integrals (meV, PBE0/DZP) for parent rubrene and derivatives (**1h** and **1k–o**) for dimer models PD, TPD1, TPD2, HD, THD, SHD, and SPD.

and derivatives (**1h** and **1k–o**) are presented in Figures S19 and S20. The PD conformation incorporating two monomers with planar tetracene backbones has the highest effective hole transfer integral. As one would expect, for both hole and

C–F···X interactions. However, substitutions at the *meta* position appear to disrupt interactions that allow for desirable crystal packing and/or prevent the planar conformation from crystallizing. We observed fluorine substituents at the *meta* position forming new C–F···X interactions in the twisted conformation, leading to alternative crystal packing motifs in the solid state.

Through our study we have demonstrated that when designing new rubrene derivatives, it is necessary to consider new intermolecular interactions that may occur, even weak C–F···X interactions. We have also observed, for the first time, a new packing motif for rubrenes: the 2-D brick, which theoretical calculations indicate could function efficiently as an organic semiconductor despite the tetracene core being in the twisted conformation. This also indicates that although planar rubrene remains ideal for maximal charge transport, planarity itself may not be critical for efficient charge transport in rubrene-based single crystal organic semiconductors. It is our hope that these findings will provide a better roadmap for the crystal engineering of π -stacked rubrene derivatives for materials science and lead to increased development of improved organic semiconductors.

■ ASSOCIATED CONTENT

Supporting Information

The Supporting Information is available free of charge on the ACS Publications website at DOI: [10.1021/acs.cgd.6b01497](https://doi.org/10.1021/acs.cgd.6b01497).

Dimer model images, tables of computed planarization energies for rubrene and derivatives, a table summarizing the crystal structures of rubrene and its derivatives presented in this work, tables defining observed interactions within different rubrene derivative crystal structures, experimental procedures for the preparation of new rubrenes with tabulated characterization data and copies of NMR spectra for new compounds, X-ray diffraction tabulated details, and transfer integrals for all dimer models, total energies, orbital pictures for dimer models and their coordinates ([PDF](#))

Accession Codes

CCDC [1509405](https://doi.org/10.1107/S0021889816004055)–[1509412](https://doi.org/10.1107/S0021889816004063) contain the supplementary crystallographic data for this paper. These data can be obtained free of charge via www.ccdc.cam.ac.uk/data_request/cif, or by emailing data_request@ccdc.cam.ac.uk, or by contacting The Cambridge Crystallographic Data Centre, 12 Union Road, Cambridge CB2 1EZ, UK; fax: +44 1223 336033.

■ AUTHOR INFORMATION

Corresponding Authors

^{*(C.J.C.)} E-mail: cramer@umn.edu. Twitter: [@ChemProfCramer](#).

^{*(L.G.)} E-mail: gagliardi@umn.edu.

^{*(C.J.D.)} E-mail: cdouglas@umn.edu.

ORCID

Christopher J. Cramer: [0000-0001-5048-1859](https://orcid.org/0000-0001-5048-1859)

Laura Gagliardi: [0000-0001-5227-1396](https://orcid.org/0000-0001-5227-1396)

Christopher J. Douglas: [0000-0002-1904-6135](https://orcid.org/0000-0002-1904-6135)

Present Addresses

[†](W.A.O.) Department of Chemistry, University of California, Irvine, 1102 Natural Sciences 2, Irvine, CA, 92697.

[§](M.J.B.) 3M Center Building 235-3-W-52 Maplewood, MN 55144.

¹(K.A.M.) Department of Chemistry, University of Wisconsin – Stevens Point, D131 Science, Stevens Point, WI 54481.

^Δ(L.B.) Department of Chemistry, McCullough Building, 476 Lomita Mall, Stanford, CA 94305.

Funding

This work was supported in part by the U.S. Department of Energy, Office of Science, Office of Basic Energy Sciences, Division of Chemical Sciences, Geosciences, and Biosciences and the Office of Advanced Scientific Computing Research through the Scientific Discovery through Advanced Computing (SciDAC) program under Award Number DE-SC0008666. The National Science Foundation is acknowledged for support via the MRSEC Program (DMR-1006566) and for a grant to purchase the Bruker-AXS D8 Venture single crystal diffractometer (MRI-1229400), along with the University of Minnesota.

Notes

The authors declare no competing financial interest.

■ ACKNOWLEDGMENTS

The authors thank Dr. Samuel Odoh for helpful discussions. The authors acknowledge the Minnesota Supercomputing Institute (MSI) at the University of Minnesota for providing resources that contributed to the research results reported within this paper. W.B.O. and L.B. thank the University of Minnesota for Undergraduate Research Opportunities Program (UROP) awards. C.J.D. thanks DuPont for a Young Professor Award.

■ REFERENCES

- (1) Desiraju, G. R. *J. Am. Chem. Soc.* **2013**, *135*, 9952–9967.
- (2) Yassar, A. *Polym. Sci., Ser. C* **2014**, *56*, 4–19.
- (3) Coropceanu, V.; Cornil, J.; da Silva Filho, D. A.; Olivier, Y.; Silbey, R.; Brédas, J.-L. *Chem. Rev.* **2007**, *107*, 926–952.
- (4) Mei, J.; Diao, Y.; Appleton, A. L.; Fang, L.; Bao, Z. *J. Am. Chem. Soc.* **2013**, *135*, 6724–6746.
- (5) Anthony, J. E.; Brooks, J. S.; Eaton, D. L.; Parkin, S. R. *J. Am. Chem. Soc.* **2001**, *123*, 9482–9483.
- (6) Ryno, S. M.; Risko, C.; Brédas, J.-L. *J. Am. Chem. Soc.* **2014**, *136*, 6421–6427.
- (7) Anthony, J. E. *Chem. Rev.* **2006**, *106*, 5028–5048.
- (8) Anthony, J. E.; Facchetti, A.; Heeney, M.; Marder, S. R.; Zhan, X. *Adv. Mater.* **2010**, *22*, 3876–3892.
- (9) Tang, M. L.; Oh, J. H.; Reichardt, A. D.; Bao, Z. *J. Am. Chem. Soc.* **2009**, *131*, 3733–3740.
- (10) Tang, M. L.; Reichardt, A. D.; Wei, P.; Bao, Z. *J. Am. Chem. Soc.* **2009**, *131*, 5264–5273.
- (11) Tang, M. L.; Reichardt, A. D.; Miyaki, N.; Stoltzenberg, R. M.; Bao, Z. *J. Am. Chem. Soc.* **2008**, *130*, 6064–6065.
- (12) Tang, M. L.; Okamoto, T.; Bao, Z. *J. Am. Chem. Soc.* **2006**, *128*, 16002–16003.
- (13) Black, H. T.; Perepichka, D. F. *Angew. Chem., Int. Ed.* **2014**, *53*, 2138–2142.
- (14) Sherman, J. B.; Moncino, K.; Baruah, T.; Wu, G.; Parkin, S. R.; Purushothaman, B.; Zope, R.; Anthony, J.; Chabinyc, M. L. *J. Phys. Chem. C* **2015**, *119*, 20823–20832.
- (15) Payne, M. M.; Parkin, S. R.; Anthony, J. E. *J. Am. Chem. Soc.* **2005**, *127*, 8028–8029.
- (16) Wang, C.; Dong, H.; Li, H.; Zhao, H.; Meng, Q.; Hu, W. *Cryst. Growth Des.* **2010**, *10*, 4155–4160.
- (17) Ye, Q.; Chi, C. *Chem. Mater.* **2014**, *26*, 4046–4056.
- (18) Sakamoto, Y.; Suzuki, T.; Kobayashi, M.; Gao, Y.; Fukai, Y.; Inoue, Y.; Sato, F.; Tokito, S. *J. Am. Chem. Soc.* **2004**, *126*, 8138–8140.

- (19) Dou, J.-H.; Zheng, Y.-Q.; Yao, Z.-F.; Lei, T.; Shen, X.; Luo, X.-Y.; Sun, J.; Zhang, S.-D.; Ding, Y.-F.; Han, G.; Yi, Y.; Wang, J.-Y.; Pei, J.; Yu, Z.-A. *J. Am. Chem. Soc.* **2015**, *137*, 15947–15956.
- (20) Ryno, S. M.; Risko, C.; Brédas, J.-L. *J. Am. Chem. Soc.* **2014**, *136*, 6421–6427.
- (21) Panini, P.; Chopra, D. Understanding of Noncovalent Interactions Involving Organic Fluorine. In *Hydrogen Bonded Supramolecular Structures*, Lecture Notes in Chemistry 87; Springer: Heidelberg, 2015; pp 37–67.
- (22) Chopra, D.; Guru Row, T. N. *CrystEngComm* **2011**, *13*, 2175–2186.
- (23) Reichenbächer, K.; Süss, H. I.; Hulliger, J. *Chem. Soc. Rev.* **2005**, *34*, 22–30.
- (24) Choudhury, A. R.; Guru Row, T. N. *Cryst. Growth Des.* **2004**, *4*, 47–52.
- (25) Rybalova, T. V.; Bagryanskaya, I. Y. *J. Struct. Chem.* **2009**, *50*, 741–753.
- (26) Schwarzer, A.; Weber, E. *Cryst. Growth Des.* **2008**, *8*, 2862–2874.
- (27) Chopra, D. *Cryst. Growth Des.* **2012**, *12*, 541–546.
- (28) Taylor, R. *Cryst. Growth Des.* **2016**, *16*, 4165–4168.
- (29) Taylor, R. *CrystEngComm* **2014**, *16*, 6852–6865.
- (30) Osuna, R. M.; Hernández, V.; Navarrete López, J. T.; D’Oria, E.; Novoa, J. *J. Theor. Chem. Acc.* **2011**, *128*, 541–553.
- (31) Panini, P.; Chopra, D. *CrystEngComm* **2013**, *15*, 3711–3733.
- (32) Podzorov, V.; Menard, E.; Borissov, A.; Kiryukhin, V.; Rogers, J. A.; Gershenson, M. E. *Phys. Rev. Lett.* **2004**, *93*, 086602/1–4.
- (33) Takeya, J.; Yamagishi, M.; Tominari, Y.; Hirahara, R.; Nakazawa, Y.; Nishikawa, T.; Kawase, T.; Shimoda, T.; Ogawa, S. *Appl. Phys. Lett.* **2007**, *90*, 102120.
- (34) Xie, W.; McGarry, K. A.; Liu, F.; Wu, Y.; Ruden, P. P.; Douglas, C. J.; Frisbie, C. D. *J. Phys. Chem. C* **2013**, *117*, 11522–11529.
- (35) Xie, W.; Prabhunirashi, P. L.; Nakayama, Y.; McGarry, K. A.; Geier, M. L.; Uragami, Y.; Mase, K.; Douglas, C. J.; Ishii, H.; Hersam, M. C.; Frisbie, C. D. *ACS Nano* **2013**, *7*, 10245–10256.
- (36) Mullenbach, T. K.; McGarry, K. A.; Luhman, W. A.; Douglas, C. J.; Holmes, R. J. *Adv. Mater.* **2013**, *25*, 3689–3693.
- (37) da Silva Filho, D. A.; Kim, E. G.; Brédas, J.-L *Adv. Mater.* **2005**, *17*, 1072–1076.
- (38) McGarry, K. A.; Xie, W.; Sutton, C.; Risko, C.; Wu, Y.; Young, V. G., Jr.; Brédas, J.-L.; Frisbie, C. D.; Douglas, C. J. *Chem. Mater.* **2013**, *25*, 2254–2263.
- (39) Paraskar, A. S.; Reddy, A. R.; Patra, A.; Wijsboom, Y. H.; Gidron, O.; Shimon, L. J. W.; Leitus, G.; Bendikov, M. *Chem. - Eur. J.* **2008**, *14*, 10639–10647.
- (40) Zhang, Z.; Ogden, W. A.; Young, V. G., Jr.; Douglas, C. J. *Chem. Commun.* **2016**, *52*, 8127–8130.
- (41) Mamada, M.; Katagiri, H.; Sakanoue, T.; Tokito, S. *Cryst. Growth Des.* **2015**, *15*, 442–448.
- (42) Bergantin, S.; Moret, M. *Cryst. Growth Des.* **2012**, *12*, 6035–6041.
- (43) Huang, L.; Liao, Q.; Shi, Q.; Fu, H.; Ma, J.; Yao, J. *J. Mater. Chem.* **2010**, *20*, 159–166.
- (44) Cozzi, F.; Ponzini, F.; Annunziata, R.; Cinquini, M.; Siegel, J. S. *Angew. Chem., Int. Ed. Engl.* **1995**, *34*, 1019–1020.
- (45) Cozzi, F.; Siegel, J. S. *Pure Appl. Chem.* **1995**, *67*, 683–689.
- (46) Hunter, C. A. *Angew. Chem., Int. Ed. Engl.* **1993**, *32*, 1584–1586.
- (47) Cozzi, F.; Cinquini, M.; Annunziata, R.; Siegel, J. S. *J. Am. Chem. Soc.* **1993**, *115*, 5330–5331.
- (48) Cozzi, F.; Cinquini, M.; Annunziata, R.; Dwyer, T.; Siegel, J. S. *J. Am. Chem. Soc.* **1992**, *114*, 5729–5733.
- (49) Sutton, C.; Marshall, M. S.; Sherrill, C. D.; Risko, C.; Brédas, J.-L. *J. Am. Chem. Soc.* **2015**, *137*, 8775–8782.
- (50) Balodis, K. A.; Medne, R. S.; Neiland, O. Y.; Kozlova, L. M.; Klyavinya, Z. P.; Mazheika, I. B.; Gaukhman, A. P. *Zh. Org. Khim.* **1985**, *21*, 2423–2427.
- (51) Yagodkin, E.; McGarry, K. A.; Douglas, C. J. *Org. Prep. Proced. Int.* **2011**, *43*, 360–363.
- (52) Yagodkin, E.; Xia, Y.; Kalihari, V.; Frisbie, C. D.; Douglas, C. J. *Phys. Chem. C* **2009**, *113*, 16544–16548.
- (53) Rowland, R. S.; Taylor, R. *J. Phys. Chem.* **1996**, *100*, 7384–7391.
- (54) Wolff, S. K.; Grimwood, D. J.; McKinnon, J. J.; Turner, M. J.; Jayatilaka, D.; Spackman, M. A. *CrystalExplorer* (Version 3.1); University of Western Australia: Crawley, Australia, 2012.
- (55) Zhao, Y.; Truhlar, D. G. *J. Chem. Phys.* **2006**, *125*, 194101.
- (56) Zhao, Y.; Truhlar, D. G. *Theor. Chem. Acc.* **2008**, *120*, 215–241.
- (57) Chai, J. D.; Gordon, M. H. *J. Chem. Phys.* **2008**, *128*, 084106.
- (58) Frisch, M. J.; Trucks, G. W.; Schlegel, H. B.; Scuseria, G. E.; Robb, M. A.; Cheeseman, J. R.; Scalmani, G.; Barone, V.; Mennucci, B.; Petersson, G. A.; Nakatsuji, H.; Caricato, M.; Li, X.; Hratchian, H. P.; Izmaylov, A. F.; Bloino, J.; Zheng, G.; Sonnenberg, J. L.; Hada, M.; Ehara, M.; Toyota, K.; Fukuda, R.; Hasegawa, J.; Ishida, M.; Nakajima, T.; Honda, Y.; Kitao, O.; Nakai, H.; Vreven, T.; Montgomery, J. A.; Peralta, Jr., J. E.; Ogliaro, F.; Bearpark, M.; Heyd, J.; Brothers, E.; Kudin, K. N.; Staroverov, V. N.; Kobayashi, R.; Normand, J.; Raghavachari, K.; Rendell, A.; Burant, J. C.; Iyengar, S. S.; Tomasi, J.; Cossi, M.; Rega, N.; Millam, J. M.; Klene, M.; Knox, J. E.; Cross, J. B.; Bakken, V.; Adamo, C.; Jaramillo, J.; Gomperts, R.; Stratmann, R. E.; Yazyev, O.; Austin, A. J.; Cammi, R.; Pomelli, C.; Ochterski, J. W.; Martin, R. L.; Morokuma, K.; Zakrzewski, V. G.; Voth, G. A.; Salvador, P.; Dannenberg, J. J.; Dapprich, S.; Daniels, A. D.; Farkas, O.; Foresman, J. B.; Ortiz, J. V.; Cioslowski, J.; Fox, D. J. *Gaussian 09*; Gaussian, Inc.: Wallingford, CT, 2009.
- (59) Perdew, J. P.; Burke, K.; Ernzerhof, M. *Phys. Rev. Lett.* **1996**, *77*, 3865–3868.
- (60) Grimme, S.; Antony, J.; Ehrlich, S.; Krieg, H. *J. Chem. Phys.* **2010**, *132*, 154104.
- (61) Chai, J. D.; Head-Gordon, M. *Phys. Chem. Chem. Phys.* **2008**, *10*, 6615–6620.
- (62) Adamo, C.; Barone, V. *J. Chem. Phys.* **1999**, *110*, 6158–6170.
- (63) Kirkpatrick, J. *Int. J. Quantum Chem.* **2008**, *108*, 51–56.
- (64) Senthilkumar, K.; Grozema, F. C.; Bickelhaupt, F. M.; Siebbeles, L. D. A. *J. Chem. Phys.* **2003**, *119*, 9809–9817.
- (65) te Velde, G.; Bickelhaupt, F. M.; Baerends, E. J.; Fonseca Guerra, C.; van Gisbergen, S. J. A.; Snijders, J. G.; Ziegler, T. *J. Comput. Chem.* **2001**, *22*, 931–967.
- (66) Dodge, J. A.; Bain, J. D.; Chamberlin, A. R. *J. Org. Chem.* **1990**, *55*, 4190–4198.
- (67) Moureu, C.; Dufraisse, C.; Dean, P. M. C. *R. Hebd. Seances Acad. Sci.* **1926**, *182*, 1440–1443.
- (68) Dufraisse, C.; Velluz, L. *Acad. Sci.* **1935**, *201*, 1394.
- (69) Braga, D.; Jaafari, A.; Miozzo, L.; Moret, M.; Rizzato, S.; Papagni, A.; Yassar, A. *Eur. J. Org. Chem.* **2011**, *2011*, 4160–4169.
- (70) McGarry, K. A. *Synthesis and Crystal Design of Rubrene Derivatives for Use in Organic Electronics*. Ph.D. Dissertation, University of Minnesota, Minneapolis, MN, 2013.
- (71) Stork, G.; Danheiser, R. L.; Ganem, B. *J. Am. Chem. Soc.* **1973**, *95*, 3414–3415.
- (72) Odom, S. A.; Parkin, S. R.; Anthony, J. E. *Org. Lett.* **2003**, *5*, 4245–4248.
- (73) Chernega, A. N.; Graham, A. J.; Green, M. L. H.; Haggitt, J.; Lloyd, J.; Mehner, C. P.; Metzler, N.; Souter, J. *J. Chem. Soc., Dalton Trans.* **1997**, 2293–2304.
- (74) Jackson, N. E.; Kohlstedt, K. L.; Savoie, B. M.; de la Cruz, M. O.; Schatz, G. C.; Chen, L. X.; Ratner, M. A. *J. Am. Chem. Soc.* **2015**, *137*, 6254–6262.
- (75) Zhang, C.; Zang, Y.; Gann, E.; McNeill, C. R.; Zhu, X.; Di, C.; Zhu, D. *J. Am. Chem. Soc.* **2014**, *136*, 16176–16184.
- (76) Huang, H.; Chen, Z.; Ortiz, R. P.; Newman, C.; Usta, H.; Lou, S.; Youn, J.; Noh, Y.-Y.; Baeg, K.-Y.; Chen, L. X.; Facchetti, A.; Marks, T. *J. Am. Chem. Soc.* **2012**, *134*, 10966–10973.
- (77) Welch, G. C.; Bakus, R. C., II; Teat, S. J.; Bazan, G. C. *J. Am. Chem. Soc.* **2013**, *135*, 2298–2305.
- (78) Özen, A. S.; Atilgan, C.; Sonmez, G. *J. Phys. Chem. C* **2007**, *111*, 16362–16371.
- (79) Casanova, D. *J. Chem. Theory Comput.* **2014**, *10*, 324–334.
- (80) Seebach, D. *Angew. Chem., Int. Ed. Engl.* **1990**, *29*, 1320–1367.

- (81) Mamada, M.; Katagiri, H.; Sakanoue, T.; Tokito, S. *Cryst. Growth Des.* **2015**, *15*, 442–448.
- (82) To solve the crystal structure of **1k**, both the CH₃ and CF₃ groups are to be refined in all *meta* positions with 50% occupancy at each side.
- (83) Kupcewicz, B.; Malecka, M. *Cryst. Growth Des.* **2015**, *15*, 3893–3904.
- (84) Nishio, M.; Umezawa, Y.; Honda, K.; Tsuboyama, S.; Suezawa, H. *CrystEngComm* **2009**, *11*, 1757–1788.
- (85) Takahashi, O.; Kohno, Y.; Nishio, M. *Chem. Rev.* **2010**, *110*, 6049–6076.
- (86) Hunter, C. A.; Sanders, J. K. M. *J. Am. Chem. Soc.* **1990**, *112*, 5525–5534.
- (87) A complete list of all intermolecular interactions for all rubrene derivatives can be found in the [Supporting Information Tables S4–S18](#).
- (88) Uttiya, S.; Miozzo, L.; Fumagalli, E. M.; Bergantin, S.; Ruffo, R.; Parravicini, M.; Papagni, A.; Moret, M.; Sassella, S. *J. Mater. Chem. C* **2014**, *2*, 4147–4155.
- (89) Atom numbering is based on the individual cif files.
- (90) McKinnon, J. J.; Spackman, M. A.; Mitchell, A. S. *Acta Crystallogr., Sect. B: Struct. Sci.* **2004**, *60*, 627–668.
- (91) Wade, J.; Steiner, F.; Niedzialek, D.; James, D. T.; Jung, Y.; Yun, D.; Bradley, D. D. C.; Nelson, J.; Kim, J. *J. Mater. Chem. C* **2014**, *2*, 10110–10115.
- (92) Kirsch, P.; Tong, Q.; Untenecker, H. *Beilstein J. Org. Chem.* **2013**, *9*, 2367–2373.
- (93) Soman, R.; Sujatha, S.; Arunkumar, C. *J. Fluorine Chem.* **2014**, *163*, 16–22.
- (94) Capozzi, M. A. M.; Capitelli, F.; Cardellicchio, C. *Cryst. Growth Des.* **2014**, *14*, 5442–5451.